Borehole flexural modes in anisotropic formations

Bikash K. Sinha*, Andrew N. Norris[‡], and Shu-Kong Chang*

ABSTRACT

A perturbation method of solution is an efficient way of analyzing elastic wave propagation along a borehole in anisotropic formations. The perturbation model allows us to calculate changes in the modal dispersion curves caused by the differences in elastic constants between the anisotropic formation of interest and a reference, or unperturbed, isotropic formation. The equivalent isotropic constants in the reference formation are obtained from the appropriate compressionaland shear-wave velocities for the selected propagation and polarization directions of the flexural mode. This choice of the unperturbed solution means that the required perturbation is minimal, resulting in enhanced accuracy of the perturbed solution. Computational results are presented for the dispersion curves of borehole flexural waves in a transversely isotropic (TI)

formation as a function of borehole deviation from the TI symmetry axis. In addition, radial distributions of displacement and stress fields associated with the flexural wave are obtained as a function of frequency. These provide qualitative information on the radial depth of investigation with flexural wave logging. The flexural wave excitation function is a measure of the energy that a source converts to flexural motion. We deduce an expression for the flexural wave excitation and show that its bandlimited characteristic is influenced by both the borehole diameter and formation parameters. From the dispersion curves and excitation functions, we can compute the flexural waveforms caused by a dipole source with arbitrary orientation in the borehole. In the numerical computations, we have used the unperturbed mode shapes for an equivalent isotropic medium together with the perturbed dispersion relations caused by the formation anisotropy.

INTRODUCTION

Various sources of anisotropy are encountered in geophysical prospecting. Some homogeneous rocks, such as Bakken shale and Austin chalk, may be intrinsically anisotropic over logging depths of interest (Thomsen, 1986). Anisotropy induced by formation lithology may also be encountered, arising from effects such as horizontally layered or dipping beds, provided that the smallest wavelength is much larger than the individual layer thicknesses (Backus, 1962; Berryman, 1979). Aligned fractures also give rise to anisotropy resembling that of a transversely isotropic medium.

In the past several decades, many observations of the seismic velocity anisotropy in exploration geophysics have been reported (Gassman, 1964; Levin, 1979; Crampin, 1985; Winterstein, 1986; Garmany, 1988; Kerner et al., 1989). While the P-wave anisotropy is usually small (0 to 10 percent) and may often be obscured by heterogeneity, the S-wave

anisotropy (0 to 10 percent) and the associated shear-wave birefringence at seismic frequencies may be significantly large and have been the focus of several recent papers (Leary et al., 1987; Lo et al., 1986; Ben-Menahem and Sena, 1990; Esmersoy, 1990). One reason for continued interest in the evaluation of anisotropy by shear-wave splitting is its potential application in the detection of aligned fractures, cracks, and other inclusions (Crampin, 1985; Winterstein, 1987; Esmersoy, 1990).

An acoustic source in a fluid-filled borehole generates head waves as well as borehole modes (Tsang and Rader, 1979; Kurkjian, 1985). The head waves are caused by coupling to plane waves in the formation that propagate along the borehole axis. Generally, there are three head waves for a borehole in an anisotropic formation. They correspond to the qP-, SH-, and *qSV* -waves in the formation. Kurkjian and Chang (1983) studied geometric decays of the head waves along the propagation direction excited by a dipole source and found them to be functions of frequency.

Manuscript received by the Editor July 20, 1992; revised manuscript received October 13, 1993. *Schlumberger-Doll Research, Old Quarry Road, Ridgefield, CT 06877-4108.

[†]Department of Mechanical and Aerospace Engineering, Rutgers University, Piscataway, NJ 088550909. © 1994 Society of Exploration Geophysicists. All rights reserved.

However, most of the acoustic energy propagating along the borehole is contained in the various borehole modes that are excited by the source for given borehole and formation parameters. Among the lowest-order axisymmetric and flexural families of borehole modes, the Stoneley mode is generated by a monopole source whereas the flexural mode is generated by a dipole source (Kurkjian and Chang, 1986). Changes in the lowest-order flexural mode dispersion curves as a function of radial polarization direction provide a convenient means for measuring azimuthal formation anisotropy. In addition, since there are no refracted shear head waves that can be detected by receivers placed in the fluid-filled borehole, flexural wave logging is the preferred technique for the estimation of shear slowness in a slow formation (where the shear wave velocity is less than the borehole-fluid compressional velocity). An attractive feature of borehole flexural waves is that its low-frequency velocity always asymptotes to the formation shear-wave speed.

Nevertheless, only a limited amount of work has been reported to date on flexural wave logging of anisotropic formations. Much of the earlier work dealt with transversely isotropic (TI) formations with the axis of symmetry parallel to the borehole axis (White and Tongtaow, 1981; Tongtaow, 1982; Chan and Tsang, 1983; Schmitt, 1989). Subsequently, Leveille and Serriff (1989) analyzed tube waves in the low-frequency limit and obtained a borehole displacement solution caused by a horizontal point force in the case of a TI formation whose symmetry axis was normal to the borehole axis. Nicoletis et al. (1990) analyzed the tube wave phenomenon in the low-frequency limit for the same kind of formation anisotropy.

Recently, Ellefsen et al. (1991) presented a study of flexural wave dispersion curves in weakly anisotropic formations from a perturbation model that was derived from Hamilton's principle. Computational results were provided for a borehole either parallel or normal to the TI symmetry axis of fast formations (where the shear-wave velocity is larger than the borehole-fluid compressional velocity). They also considered a borehole aligned with an axis of an orthorhombic solid, for which the starting solution for the perturbation scheme is for an isotropic formation whose shear velocity is an average of the two shear velocities along the selected propagation direction. Note that in anisotropic solids, the two shear velocities corresponding to the *qSV*-and SH-polarized waves propagating along a given direction are usually different.

Additional numerical results for anisotropic formations were recently presented by Leslie and Randall (1992), who developed a finite-difference method for the computation of time-waveforms at an array of receivers because of a monopole or dipole source pulse in a fluid-filled borehole. These waveforms can be processed by a variation of Prony's algorithm (Lang et al., 1987) to yield either the Stoneley or flexural wave dispersion curves. Although this numerical procedure can handle any type of anisotropy, the accuracy and large computing time compared to those of analytical models may limit its usefulness in some cases.

Analytical modeling of wave propagation in cylindrical coordinates with the anisotropy of the medium expressed in a Cartesian reference frame provides unique challenges in writing the solution in a separable form. These challenges stem from the directional dependence of the elastic constants in an anisotropic medium when represented in cylindrical coordinates. The resulting differential equations of motion with variable coefficients do not offer straightforward solutions in a closed form.

In this paper, we present a perturbation solution method for elastic wave propagation along a borehole in an anisotropic formation. This perturbation technique readily treats spatial changes in both the elastic constants and mass density of the elastic medium and yields the corresponding changes in the frequency-wavenumber dispersion curves. Instead of working with any kind of "average" material constants, we find that the best choice of equivalent isotropic parameters for the unperturbed state are those derived from the appropriate compressional- and shear-wave velocities for the selected propagation and polarization directions. The propagation direction is the borehole axial direction, and the polarization depends upon the polarization direction of the flexural mode. This choice of equivalent isotropic parameters results in a relatively small correction to the dispersion and ensures high accuracy of the predicted dispersion curve.

Computational results are obtained for the dispersion curves for the qSV- and SH-polarized flexural waves along several orientations of a borehole in Bakken shale (a fast TI formation) and Austin chalk (a slow TI medium). Computational results are also provided for the radial distribution of modal amplitudes as a function of frequency in the Austin chalk (a slow TI formation). Of particular importance in flexural wave logging is the radial depth of investigation at a given frequency. To this end, we discuss the radial distribution of modal amplitudes as a function of frequency for qSV-polarized flexural waves along a borehole in Austin chalk when the borehole axis makes an angle of 45 degrees with the TI symmetry axis. In addition, we define an excitation amplitude function for the flexural modes and illustrate its frequency dependence along with synthetic waveforms at an array of receivers that result from a dipole source oriented along the qSV- and SH-displacement directions on the borehole axis. Since the dipole source may not always be oriented along a canonical direction of either the qS V- or SH-displacement direction, we present synthetic waveforms that result from a dipole source directed along an azimuthal angle of 30 degrees from the qSV-displacement direction in a borehole normal to the TI symmetry axis. These synthetic waveforms may be significantly different from the cases when the source is directed along either the qSV- or SH-displacement directions. This difference is a result of the flexural wave splitting into the qSV- and SH-polarized flexural waves propagating at different velocities because of the formation anisotropy. Flexural wave splitting over an intermediate frequency band may also occur because of the borehole ellipticity in an isotropic formation (Randall, 1991; Liu and Randall, 1991). However, borehole ellipticity-induced azimuthal anisotropy in flexural wave dispersion curves becomes negligibly small at both low and high frequencies. On the other hand, formation induced azimuthal anisotropy in flexural wave dispersion curves is, generally, the largest at low frequencies.

ELASTIC WAVES IN A BOREHOLE

The propagation of plane elastic waves in anisotropic solids is governed by the equations of motion, which take the following form in the absence of any body force density:

$$C_{ijk\ell} u_{k,i\ell} = \rho \ddot{u}_j, \tag{1}$$

where $C_{ijk\ell}$ and ρ are the elastic constants and mass density of the solid, respectively. In the following, we have used the Cartesian tensor notation and the convention that a comma followed by an indexj denotes differentiation with respect to x_j . The summation convention for repeated tensor indices and the dot notation for differentiation with respect to time are also implied. A plane-wave solution to equation (1) may be written

$$u_i = A_i e^{ik(n_i x_i - Vt)}, (2)$$

where n_i are the direction cosines of the wave vector with respect to the Cartesian axes x_i , k, and V are the wavenumber and phase velocity, respectively. Substitution of equation (2) into equation (1) yields (Auld, 1973)

$$(Q_{jk} - \delta_{jk}\rho V^2)A_j = 0, (3)$$

where the acoustical tensor is

$$O_{ik} = C_{ijk\ell} n_i n_\ell. \tag{4}$$

The three plane-wave velocities along a given propagation direction are obtained from the three eigenvalues of equation (4). The associated eigenvectors corresponding to each of these three eigenvalues define the wave polarization vectors. These plane-wave velocities are thus calculated along the borehole axis to determine the equivalent isotropic constants for the solution of the background medium in the perturbation model.

Next, we describe a procedure for obtaining synthetic flexural waveforms resulting from a dipole source in anisotropic formations. To this end, we first consider transient solutions of the borehole modes with an impulsive source located in the liquid-filled cylindrical borehole. The forced equations of motion describing such transient solutions may be written as

$$\mathcal{L}\mathbf{u}(r,\,\mathbf{\Phi},\,z,\,t) - \mathbf{\rho}\ddot{\mathbf{u}} = -\mathbf{F}(r,\,\mathbf{\Phi},\,z,\,t),\tag{5}$$

where \mathcal{L} is a linear operator, and F is a forcing function. A partial solution (see discussion below) to equation (5) may be expressed in terms of a summation over the eigenfunctions of the operator \mathcal{L} . The borehole and formation are assumed to be independent of the axial coordinate, implying that it is convenient to use eigenfunctions in the form of vertical transforms. Accordingly, we generalize the preceding analysis to include the associated complex-valued eigenfunctions. The modal sum becomes

$$\mathbf{u}(r,\,\phi,\,z,\,t) = \operatorname{Re} \sum_{m} \int_{0}^{\infty} \mathbf{u}^{m}(r,\,\phi,\,z,\,k) q_{m}(t,\,k) \,\,dk, \tag{6}$$

where $q_m(t, k)$ are the modal weighting functions to be determined for a given forcing function, and the index m

represents the mth eigenfunction of the operator \mathcal{L} . The complex-valued eigenfunction \mathbf{u}^m satisfies the equation

$$\mathcal{L}\mathbf{u}^m + \rho \omega_m^2 \mathbf{u}^m = 0, \tag{7}$$

and is assumed to be of the form

$$\mathbf{u}^{m}(r, \, \mathbf{\varphi}, \, z, \, k) = \mathbf{U}^{m}(r, \, \mathbf{\varphi}, \, k)e^{ikz}. \tag{8}$$

The modal frequency is therefore a function of the vertical wavenumber, i.e., the modal dispersion relationship may be expressed as

$$\omega_m = \omega_m(k). \tag{9}$$

Next, we define Fourier transform pairs as

$$\hat{\mathbf{F}}(r, \, \phi, \, t, \, k) = \int_{-\infty}^{\infty} \mathbf{F}(r, \, \phi, \, z, \, t) e^{-ikz} \, dz, \qquad (10)$$

and

$$\mathbf{F}(r, \, \phi, \, z, \, t) = \frac{1}{\pi} \operatorname{Re} \, \int_0^{\infty} \hat{\mathbf{F}}(r, \, \phi, \, t, \, k) e^{ikz} \, dk. \tag{11}$$

Substituting from equation (6) into equation (5) and with the aid of equations (8) and (9), we obtain

$$\sum_{m} \rho [\ddot{q}_{m}(t, k) + \omega_{m}^{2} q_{m}(t, k)] \mathbf{U}^{m}(r, \phi, k)$$

$$= \frac{1}{\pi} \hat{\mathbf{F}}(r, \phi, t, k). \quad (12)$$

Taking the inner product of equation (12) with $\mathbf{U}^m * (r, \phi, k)$ and using the orthogonality conditions, we obtain uncoupled equations for the modal amplitude functions, which have the form

$$\ddot{q}_m(t, k) + \omega_m^2 q_m(t, k) = \frac{\hat{F}^m(t, k)}{\pi M^m(k)},$$
 (13)

where

$$M^{m}(k) = \int_{0}^{2\pi} d\phi \int_{0}^{\infty} r dr \rho \mathbf{U}^{m*} \cdot \mathbf{U}^{m}, \qquad (14)$$

* denotes complex conjugate, and

$$\hat{F}^{m}(t, k) = \int_{0}^{2\pi} d\phi \int_{0}^{\infty} r \, dr \, \hat{\mathbf{F}}(r, \phi, t, k) \cdot \mathbf{U}^{m*}(r, \phi, k),$$
(15)

The solution to equation (13) follows from a standard procedure based on Laplace transform technique and can be expressed in terms of a convolution integral (Sneddon, 195 1). Assuming that the forcing is zero for t < 0, we have

$$q_m(t, k) = \frac{H(t)}{\omega_m \pi M^m} \int_0^t \hat{F}^m(\tau, k) \sin \omega_m(t - \tau) d\tau,$$
(16)

where H(t) is the Heaviside function. For simplicity, we consider a point force on the borehole axis,

$$\mathbf{F}(r, \, \phi, \, z, \, t) = \mathbf{F}_0(t) \, \frac{\delta(r)}{2\pi r} \, \delta(z),$$

$$\hat{\mathbf{F}}(r, \, \phi, \, t, \, k) = \mathbf{F}_0(t) \, \frac{\delta(r)}{2\pi r}. \tag{17}$$

Here, $\mathbf{F}_0(t)$ is the point force vector, with units of force. Substituting for the weighting function $q_m(t, k)$ into equation (6), the time-domain solution for the particle displacement caused by the impulsive force on the borehole axis at t = 0, may be expressed as

$$\mathbf{u}(r, \, \phi, \, z, \, t) = \frac{H(t)}{\pi} \operatorname{Re} \sum_{m} \times \int_{0}^{\infty} \frac{dk e^{ikz}}{\omega_{m} M^{m}(k)} \, \mathbf{U}_{m}(r, \, \phi, \, k)$$

$$\times \int_0^t \left[\mathbf{F}_0(\tau) . \mathbf{U}^{m*}(0, k) \right] \sin \omega_m(k) (t - \tau) d\tau. \tag{18}$$

Equation (18) represents a time-domain solution in terms of a wavenumber integral. The procedure for obtaining a solution for borehole modes in the frequency-domain in terms of their dispersion characteristics is explained in Appendices A, B, and C. Once the wavenumber-frequency relationship is known via the dispersion curve, we can transform equation (18) into a more illuminating frequency integral that clearly shows the convolution of the flexural mode spectrum \mathbf{U}^m (0, k_m (w)) and source spectrum $\mathbf{F}_0(\omega)$. The resulting expression takes the form

$$\mathbf{u}(r, \, \phi, \, z, \, t) = \frac{H(t)}{\pi} \operatorname{Re} \sum_{m} \times \int_{0}^{\infty} \frac{d\omega \, e^{ik_{m}(\omega)z}}{M^{m}(k_{m}(\omega))C_{g}^{m}(\omega)}$$

$$\times \left[\mathcal{F}_0(\omega) \cdot \mathbf{U}^{m*}(0, k_m(\omega)) \right] \mathbf{U}^m(r, \phi, k_m(\omega)) \frac{\sin \omega t}{\omega}, \tag{19}$$

where $k_m = k_m(\omega)$ is the inverse of equation (9), and the modal group velocity $C_q^m(\omega)$ is

$$C_g^m(\omega) = \frac{d\omega_m(k)}{dk}.$$
 (20)

The function $\mathcal{F}_0(\omega)$ in equation (19) is the transform of the forcing function, defined as

$$\mathcal{F}_0(\omega) = \int_0^\infty \mathbf{F}_0(t)e^{i\omega t} dt. \tag{21}$$

Appendix D contains a derivation of the source spectrum $\mathcal{F}_0(\omega)$ for a dipole source placed on the axis of a fluid-filled borehole

The preceding analysis is exact for a system that can be described completely by a discrete spectrum of modes. If the

formation were of finite radius, rather than infinite, then the modes of the borehole plus formation would indeed be discrete. However, the infinite radial extent of the formation means that there are continuous spectrum contributions. In the isotropic case these correspond to the branch line integrals for the P- and S-waves, and manifest themselves physically as head waves. Similar head wave effects can be expected in the anisotropic formation, and these must be added to the modal expansion to provide the complete solution. However, unlike the borehole modes, the head waves decay with distance along the borehole (Kurkjian and Chang, 1983), and may be safely ignored at relatively large source-receiver separations. In the numerical results reported here, we have not included any head wave effects, but just used the modal expansion in equation (19).

In applying equation (19) to anisotropic formations, it is necessary to know both the dispersion relations and the mode shapes for each term in the series. However, for *small* anisotropy the dispersion relation can be approximated well by the perturbation theory described in Appendices A and B. The mode shapes may be determined by a similar type of asymptotic analysis. However, it can be easily shown that the change in the mode shape is of order ε^2 and is therefore of less significance than the change in the dispersion curve. In the numerical computations we have used the unperturbed mode shapes combined with the perturbed dispersion relations.

Referring to equation (19), the modal amplitude of the radial component of the particle acceleration on the borehole axis may be defined as

$$A_r^m(\omega, \phi) = \frac{\omega^2 |\mathbf{e}^r 1 \mathbf{U}^m(0, k_m)|^2}{M^m(k_m) C_q^m},$$
 (22)

where \mathbf{e}^r is a unit vector along the radial direction associated with the direction of the dipole that excites the flexural wave (see Appendix D). This quantity measures the coupling of a dipole to mode m, and its frequency dependence is of some significance. We note that the normalization parameter M^m can be obtained in closed form from Appendix C.

Since we are interested in obtaining synthetic waveforms exclusively caused by either the qSV- or SH-polarized flexural modes, only one term in equations (18) or (19) contains the flexural wave solution, and the summation over the index m is not needed. The polarization direction for the flexural mode (m=1) is along the $\phi=0$ direction, where ϕ is the azimuthal angle in the plane perpendicular to the borehole. The frequency dependence of A_r^m indicates the excitation potential of the mth mode as a function of frequency of the dipole source. The dipole source spectrum $\mathcal{F}_0(\omega)$ employed in this study is given by the second-derivative of the Blackman-Harris window and is described in Kurkjian and Chang (1986).

It is assumed for the remainder of the paper that the formation is transversely isotropic with its axis of symmetry aligned in an arbitrary direction relative to the borehole, as shown in Figure 1. Given the borehole axis as the propagation direction, there are two canonical (or principal) directions in the plane normal to it that correspond to the SH- and qSV-wave polarizations in the formation. Specifically, when the TI symmetry (x_3) axis is normal to the borehole (x_2)

axis, the *SH*- and *qSV-wave* polarizations are oriented along the x_1 and x_3 directions, respectively. Assuming that the dipole transmitter is oriented at an azimuthal angle ψ from the symmetry axis, the radial component of the flexural waveforms \mathbf{u}^{inline} and $\mathbf{u}^{crossline}$ at the inline and crossline receivers, respectively, are given by

$$\mathbf{u}^{inline} = \mathbf{u}^{SH} \sin^2 \psi + \mathbf{u}^{SV} \cos^2 \psi, \tag{23}$$

and

$$\mathbf{u}^{crossline} = \frac{1}{2} (\text{"SH} - \mathbf{u}^{SV}) \sin 2\psi, \tag{24}$$

where \mathbf{u}^{SH} and \mathbf{u}^{SV} are, respectively, given by equation (19) with all the quantities referred to the appropriate solutions for the SH- or SV-polarized flexural waves at a given frequency $\boldsymbol{\omega}$. It is clear from these results that there will not be any flexural arrivals at the crossline receivers when the dipole transmitter orientation $\boldsymbol{\psi}$ is either 0 degree or 90 degrees.

COMPUTATIONAL RESULTS

A schematic of a borehole of radius a inclined at an angle θ with respect to the TI symmetry axis is shown in Figure 1. Since the measurements are performed along the borehole axis, the TI elastic constants of the formation are initially expressed with respect to the unprimed x_1 , x_2 , and x_3 axes,

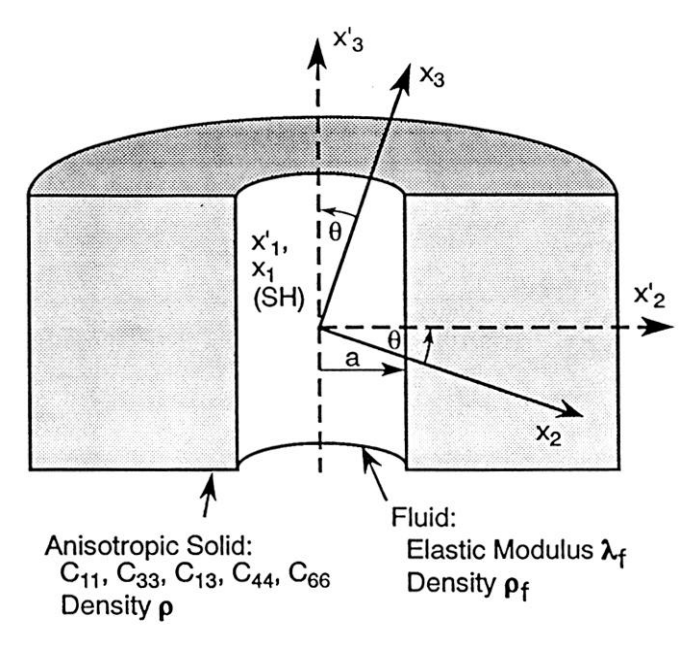


FIG. 1. Schematic diagram of a fluid-filled borehole. The borehole axis makes an angle θ with the TI symmetry axis.

where x_3 is coincident with the TI symmetry axis. These constants are then transformed into rotated constants referred to the primed x'_1 , x'_2 , and $x'_3 \equiv z$ axes for the case when the borehole axis makes an angle θ with the TI symmetry axis (Auld, 1973). The resulting elastic constants referred to the rotated axes exhibiting monoclinic symmetry. However, it is worth noting that those elastic constants, C_{14} , C_{24} , C_{34} , and C_{56} , which couple the normal stresses and shear strains, do not have any influence on the flexural wave dispersion curves since all the perturbation integrals associated with them vanish (see Appendix B). Note that in this example the elastic constants possess monoclinic symmetry, with $x_1 = x'_1$ as the binary axis. That is, the material constants exhibit 180 degrees rotational symmetry about the x_1 axis. Nevertheless, the same elastic constants do produce coupling between the flexural and axisymmetric Stoneley waves along the borehole.

To illustrate the application of the perturbation model to predict the flexural wave propagation characteristics in a liquid-filled borehole in an anisotropic formation, we present results for the qSV- and SH-polarized flexural wave dispersion curves for various inclinations with respect to the TI symmetry axis for two types of formations: (I) Bakken shale, a fast TI formation and (2) Austin chalk, a slow TI formation. A fast formation implies that both the qSV- and SH-wave velocities are higher than the compressional-wave velocity in the borehole fluid; whereas in a slow formation, both shear-wave velocities are lower than the borehole fluid velocity.

When referred to the Cartesian axes (x_1, x_2, x_3) , with x_3 as the TI symmetry axis, the mass density and elastic moduli for Bakken shale (Vernik and Nur, 1991) and Austin chalk (White, 1983) are shown in Table I. The borehole liquid is assumed to have a compressional speed of 1500 m/s and mass density of 1000 kg/m³. All computational results are for a borehole of radius IO.16 cm (4 inches).

Figures 2a and 2b, respectively, show qP-, and qSV- and SH-wave velocities in Bakken shale as a function of propagation direction from the TI symmetry axis. The corresponding wave velocities in Austin chalk are displayed in Figures 3a and 3b, respectively. Note the significant difference in the variation of qSV-wave velocity with the propagation direction in these two cases. These velocities play an extremely important role in obtaining the dispersion curves for the borehole surrounded by an anisotropic formation. For given propagation and polarization directions, they provide parameters for an equivalent isotropic medium corresponding to either qP- and qSV-velocities or qP- and SH-velocities. As part of an illustration, consider the propagation of flexural waves along the borehole axis that make an angle $\theta = 26$ degrees with the TI symmetry axis for the

Table 1. Model parameters.

$\rho (kg/m^3)$	$C_{11} \text{ N/m}^2$	$C_{12} \text{ N/m}^2$	$C_{13} \text{ N/m}^2$	$C_{33} \text{ N/m}^2$	$C_{44} \text{ N/m}^2$
Bakken shale 2230	40.9×10^{9}	10.3×10^{9}	8.5×10^{9}	26.9×10^{9}	10.5×10^{9}
Austin chalk 2200	22.0×10^9	15.8×10^{9}	12.0×10^{9}	14.0×10^{9}	2.4×10^{9}

Bakken shale formation. We can obtain exact plane-wave velocities from equations (3) and (4). These velocities are also plotted in Figures 2a and 2b. For $\theta = 26$ degrees, the plane-wave velocities in Bakken shale are: $V_{qP} = 3568.5$ m/s; $V_{qSV} = 2263.22$; and $V_{SH} = 2289.89$. The equivalent isotropic moduli, μ and λ , for the SH-polarized flexural waves along the borehole axis are given by $\mu_{SH} = \rho V_{SH}^2$, and $\lambda_{SH} = \rho (V_{qP}^2 - 2V_{SH}^2)$, and that for the qSV-polarized flexural waves are obtained from $\mu_{qSV} = \rho V_{qSV}^2$, and $\lambda_{qSV} = \rho (V_{qP}^2 - 2V_{qSV}^2)$, where the subscripts "SH" and "qSV" denote the equivalent isotropic moduli for the SHand qS V-polarized flexural waves, respectively. These equivalent isotropic parameters serve to define the flexural wave solutions in the reference or unperturbed state. Any contribution to the flexural wave dispersion curve because of the differences in the elastic moduli of the anisotropic formation and the aforementioned equivalent isotropic moduli is accounted for in the perturbation model discussed earlier. However, perturbative corrections to the flexural wave dispersion curves are rather small for the two examples considered in this paper when the equivalent isotropic moduli are obtained from the appropriate plane-wave velocities for propagation along the borehole axis.

Figures 4a and 4b illustrate the *SH*- and @V-polarized flexural wave dispersion curves, respectively, for four different inclinations of the borehole with respect to the TI symmetry axis for Bakken shale (a fast TI formation). Both the *SH*- and @V-polarized flexural wave dispersion curves tend toward the Stoneley-wave velocity at frequencies

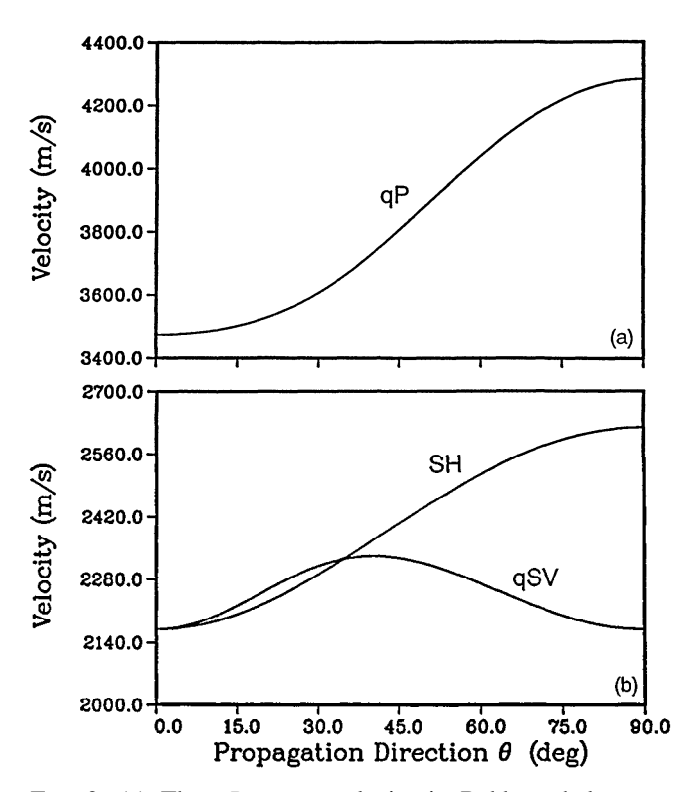


FIG. 2. (a) The qP -wave velocity in Bakken shale as a function of propagation direction from the TI symmetry axis. (b) The qSV- and SH-wave velocities in Bakken shale as a function of propagation direction from the TI symmetry axis.

higher than 10 kHz for the planar interface between the borehole liquid and anisotropic formation. Since the Stoneley-wave velocity in a fast formation is essentially close to the compressional speed in the liquid, curves for the different borehole inclinations coalesce more tightly than at lower frequencies. The corresponding curves for Austin chalk (a slow TI formation) are shown in Figures 5a and 5b, respectively, for the SH- and @V-polarized flexural waves. Unlike fast formations, both SH- and @V-polarized flexural waves in these plots exhibit a rather uniform spread at higher as well as lower frequencies. Of course, the low-frequency asymptotes of all these flexural wave dispersion curves are the corresponding shear speed in the formation; whereas the high-frequency asymptotes turn out to be the Stoneley-wave velocity appropriate for the propagation and polarization directions. Both the low- and high-frequency asymptotes of the flexural wave dispersion curves contain information about the anisotropic constants of the surrounding formation and are independent of the borehole geometry. Comparison of the perturbation model predictions of dispersion curves with those of the finite-difference results (Leslie and Randall, 1992) for Austin chalk over a band-limited window of the source pulse shows agreement in the range of 2 to 5 percent. This agreement is good in view of the coarse grid size in the finite-difference model and band-limited source pulse employed in the calculations together with possible limitations of the perturbation model in treating formations with moderately large anisotropy, such as that of Austin chalk. Although we have not included results for Cotton valley shale in this paper, a similar comparison between the perturbation model and finite-difference results (Leslie and

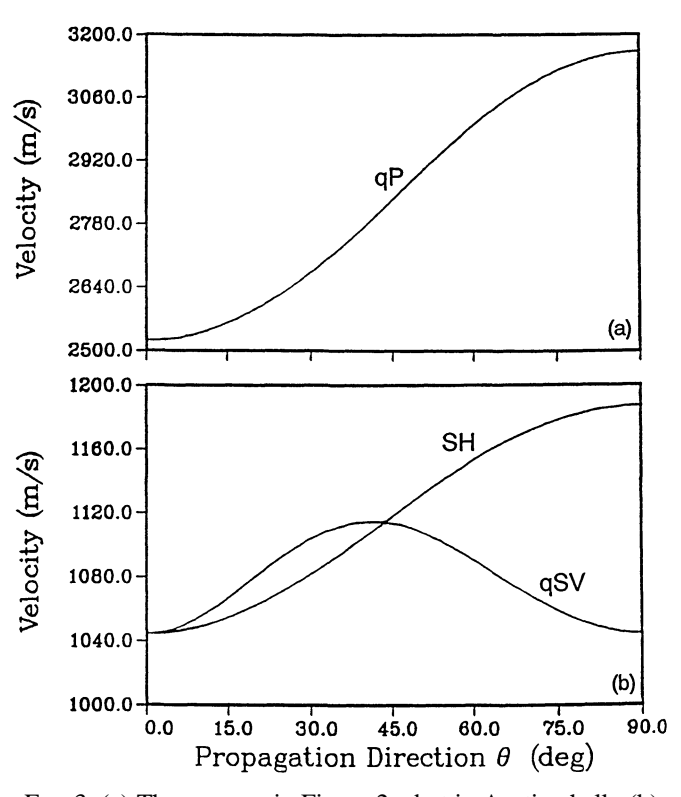


FIG. 3. (a) The same as in Figure 2a, but in Austin chalk. (b) The same as in Figure 2b, but in Austin chalk.

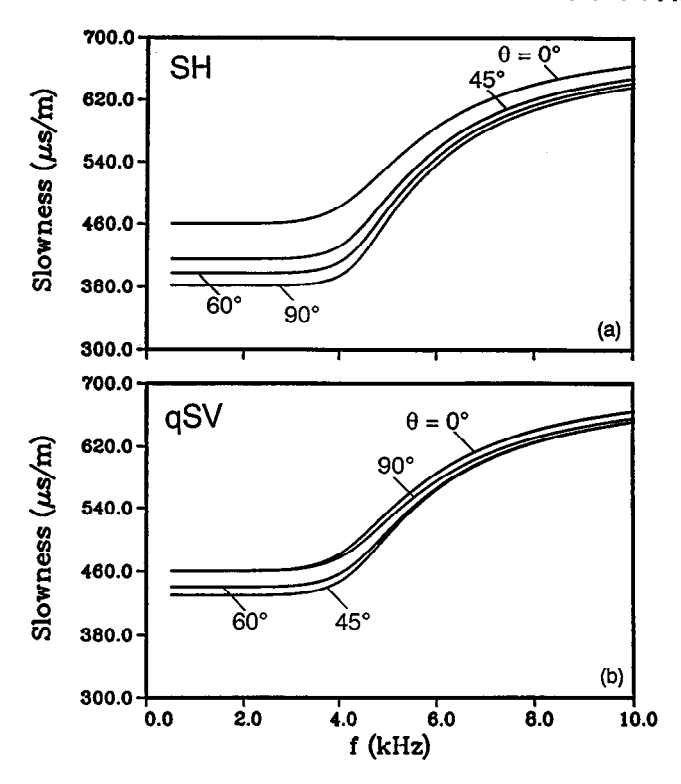


FIG. 4. (a) Phase velocity dispersion curves for S&polarized flexural waves along boreholes in Bakken shale with different inclinations θ with respect to the TI symmetry axis. (b) Phase velocity dispersion curves for qS V-polarized flexural waves along boreholes in Bakken shale with different inclinations θ with respect to the TI symmetry axis.

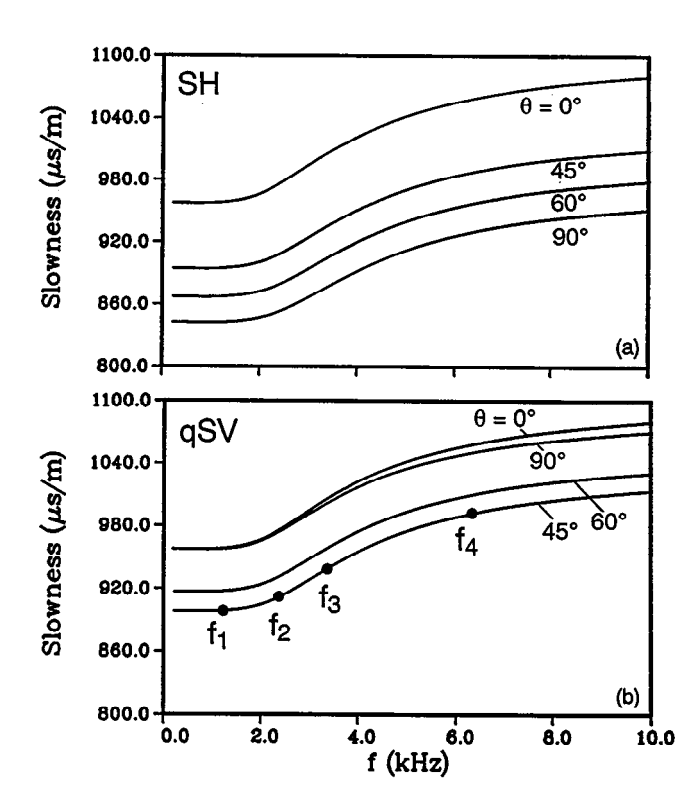


FIG. 5. (a) The same as in Figure 4a, but in Austin chalk. (b) The same as in Figure 4b, but in Austin chalk.

Randall, 1992) shows better agreement than that for Austin chalk

Radial distribution of modal amplitudes is indicative of the radial depth of investigation with flexural logging at a given frequency. To demonstrate the significant frequency dependence of the modal amplitude distribution, we present the normalized radial coefficient for the displacement and normal stress components at frequencies of 1.22, 2.24, 3.34, 6.32, and 12.3 kHz. The first four frequencies are denoted by f_1 , f_2 , f_3 , and f_4 , respectively, in Figure 5b for the borehole inclined at an angle of 45 degrees to the symmetry axis. The fifth frequency of 12.3 kHz is outside the range of Figure 5b. These results are for @V-polarized flexural waves in a soft formation represented by Austin chalk. The radial displacement and stress components are defined in Appendix B. Only the radial coefficients of the displacement and normal stresses have been plotted in Figures 6 through 10, and the quantities u_r and σ_{rr} are normalized to unity at the borehole surface given by r/a = 1.

Figures 6a and 6b, respectively, illustrate the particle displacement components u_r , u_{ϕ} , and u_z and the three normal stress components in the borehole liquid, which extend to r/a=1 and in the adjoining formation, in the region r/a>1 for the flexural mode at 1.22 kHz. To illustrate the stronger confinement to the borehole surface with increasing frequency of the flexural mode, we present

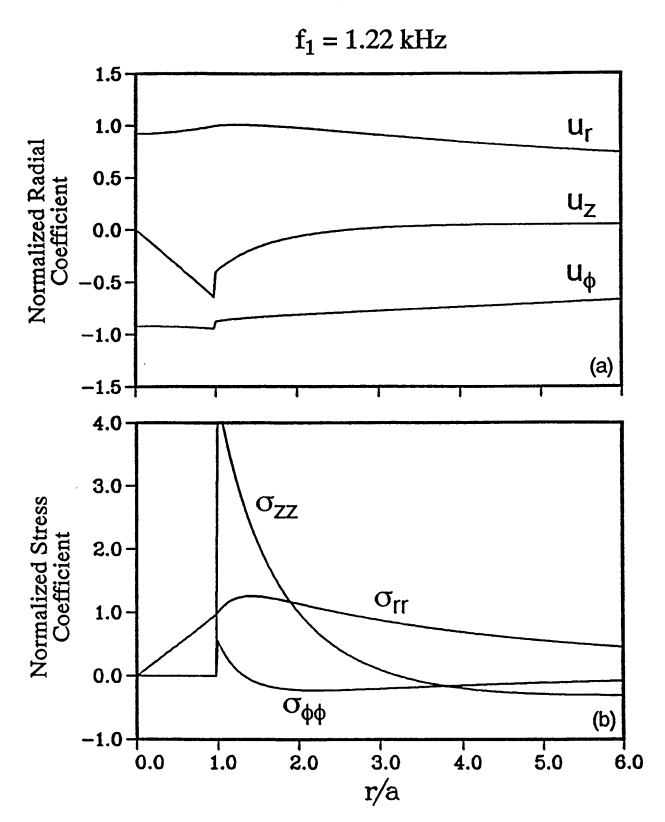


FIG. 6. (a) Radial distribution of displacement component coefficients for qSV-polarized flexural waves along a borehole inclined at an angle of 45 degrees with respect to the TI symmetry axis of Austin chalk. The borehole surface is at rla=1, and the harmonic frequency is 1.22 kHz. (b) Radial distribution of normal stress component coefficients for the flexural wave. The notation is the same as in Figure 6a.

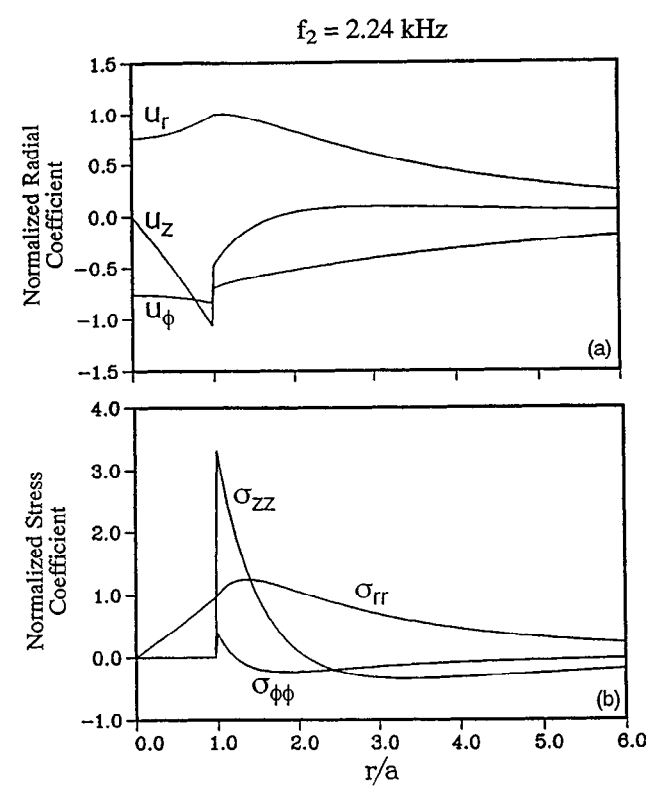


FIG. 7. (a) The same as in Figure 6a, but for the frequency of 2.34 kHz. (b) The same as in Figure 6b, but for the frequency of 2.34 kHz.

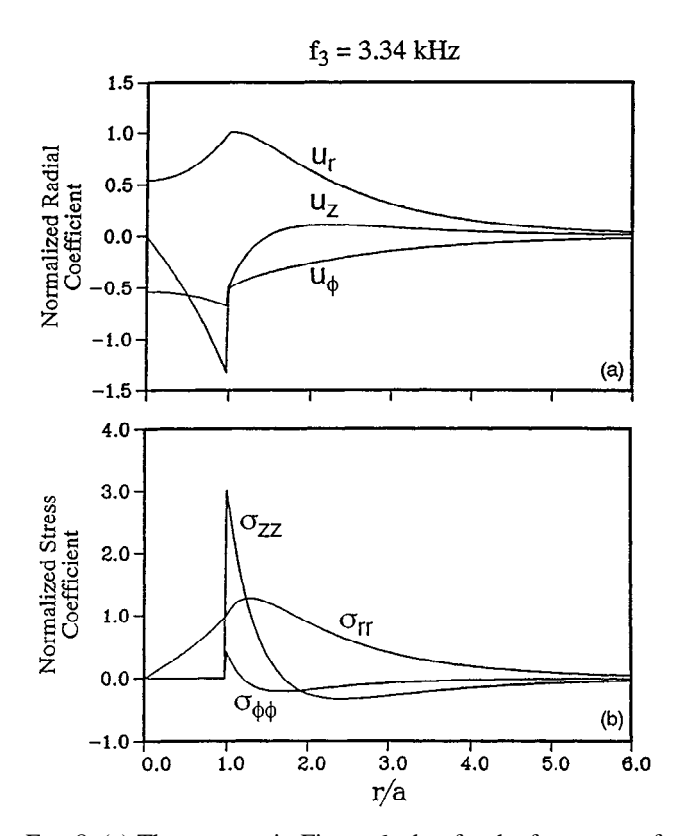


FIG. 8. (a) The same as in Figure 6a, but for the frequency of 3.34 kHz. (b) The same as in Figure 6b, but for the frequency of 3.34 kHz.

these plots in Figures 7a and 7b, 8a and 8b, 9a and 9b, and 10a and 10b for frequencies at 2.34,3.34,6.32, and 12.3 kHz, respectively. What is noteworthy in these plots is how rapidly the modal amplitudes decay away from the borehole surface with increasing frequency. This radial decay of the modal amplitudes has important implications in its potential interaction with radial inhomogeneities. In addition, it is obvious from Figures 10a and 10b that the flexural wave has almost transformed into a planar Stoneley mode at the interface between the borehole fluid and the formation at around 12 kHz.

Next, we discuss the flexural wave dispersion curves and synthetic waveforms caused by a dipole source oriented along the qSV- and SH-displacement directions in a borehole normal to the TI symmetry axis of Austin chalk. Figures Ila and Ilb, respectively, show the normalized phase and group velocities of qSV- and S&polarized flexural waves as a function of frequency. Note that these two sets of curves appear to be very similar, but the normalization factor in each case is the appropriate qSV- or SH-wave velocity. Figure 1 lc illustrates the excitation amplitude A_r^m (ω , 0) of equation (37) for the radial component of particle acceleration on the borehole axis associated with the SH- (solid line) and qSV- (dotted line) polarized flexural waves as a function of frequency. These curves may be viewed as the modal frequency spectrum, which indicates the excitation potential of the flexural mode as a function of frequency for a given borehole diameter, formation parameters and flexural polarization direction. These results are normalized with respect to the largest amplitude of the

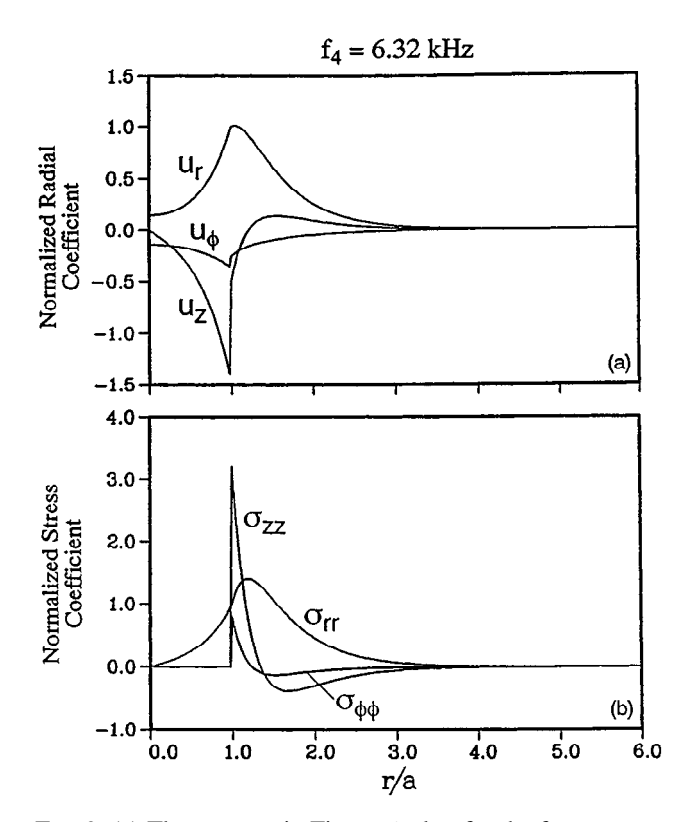


FIG. 9. (a) The same as in Figure 6a, but for the frequency or 6.32 kHz. (b) The same as in Figure 6b, but for the frequency of 6.32 kHz.

SH polarized flexural wave at about 4 kHz. Note that the SH-polarized flexural wave with higher phase velocity than that of the SV-polarized flexural wave exhibits a higher excitation level. The overall behavior of the excitation function is similar to that observed in the isotropic case.

The time waveforms for the radial acceleration component for a dipole source directed along the SH- and SV-polarization directions are shown in Figures 12a and 12b, respectively. The source spectrum is given by the second-derivative of the Blackman-Harris window (Kurkjian and Chang, 1986) and is centered at 2.5 kHz. These waveform traces have been computed at eight source-receiver offsets of z = 243.84 cm (8 ft), 259.08 (8.5), 274.32 (9), 289.56 (9.5), 304.8 (10), 320.04 (10.5), 335.28 (11), and 350.52 (11.5). Note that the waveform amplitudes are somewhat larger for the SHpolarized flexural wave than for the SV-polarized flexural wave for the same source amplitude. This difference in amplitude is a result of the difference in the modal spectra for the two flexural waves as shown in Figure 1 lc. In fact, the time waveform for the SH-polarized flexural wave is significantly larger than that of the SV-polarized flexural wave for a source pulse centered around 4 kHz.

Figure 13 shows a schematic diagram of orientation of a dipole source and inline (X-X) or crossline (X-Y) receivers in a borehole. Figures 14a and 14b, respectively, show the inline and crossline dipole receiver waveforms caused by a dipole source in a borehole normal to the TI symmetry axis

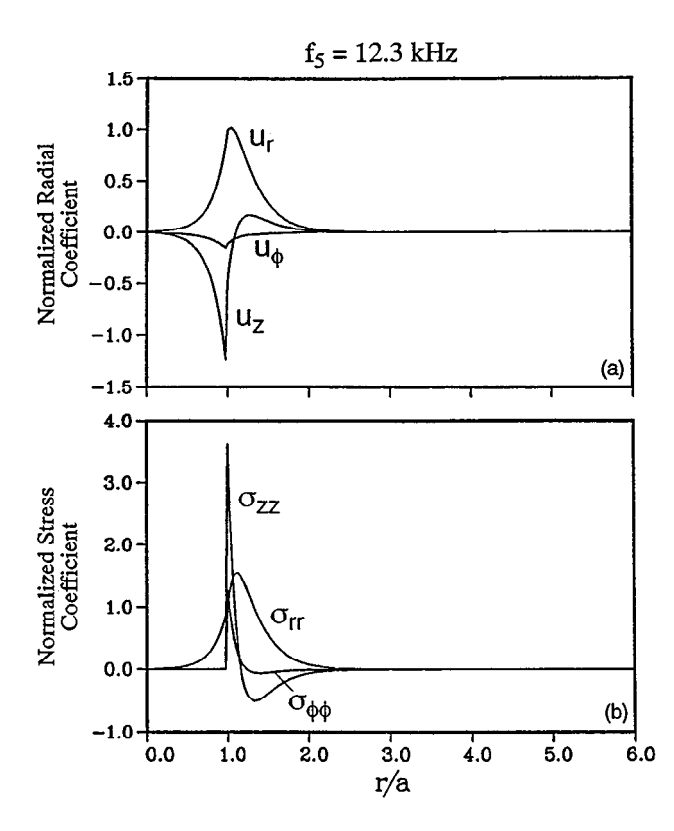


FIG. 10. (a) The same as in Figure 6a, but for the frequency of 12.3 kHz. (b) The same as in Figure 6b, but for the frequency of 12.3 kHz.

of Austin chalk and oriented at an azimuthal angle of 30 degrees from the SV-displacement direction (which coincides with the TI symmetry axis). Figure 14c shows the inline dipole receiver waveforms for a dipole that is perpendicular to the orientation of Figure 14a. The source spectrum and the source-receiver offsets are the same as those in Figures 12a and 12b. Each of these three sets of waveforms have been synthesized from the same two dispersion curves associated with the SH- and qSV-polarized flexural waves and an assumed source spectrum. The differences in the waveforms are a result of the vector decomposition of the flexural wave along the two canonical directions and the resulting interference between the SH- and qSV-polarized waves.

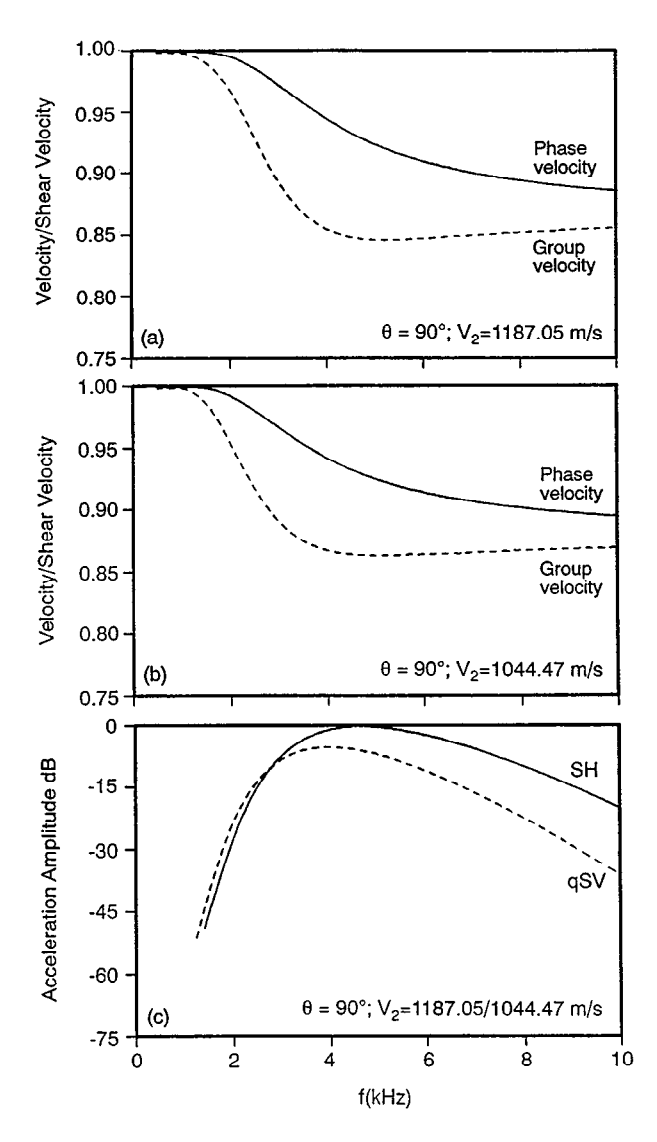


FIG. 11. (a) Normalized phase and group velocities for the SH-polarized flexural wave. Propagation direction is normal to the TI symmetry axis. (b) The same as in Figure 1 la, but for the qSV-polarized flexural wave. (c) Frequency dependence of excitation function (radial component of particle acceleration on the borehole axis) for *SH*- and *qS* V-polarized flexural waves.

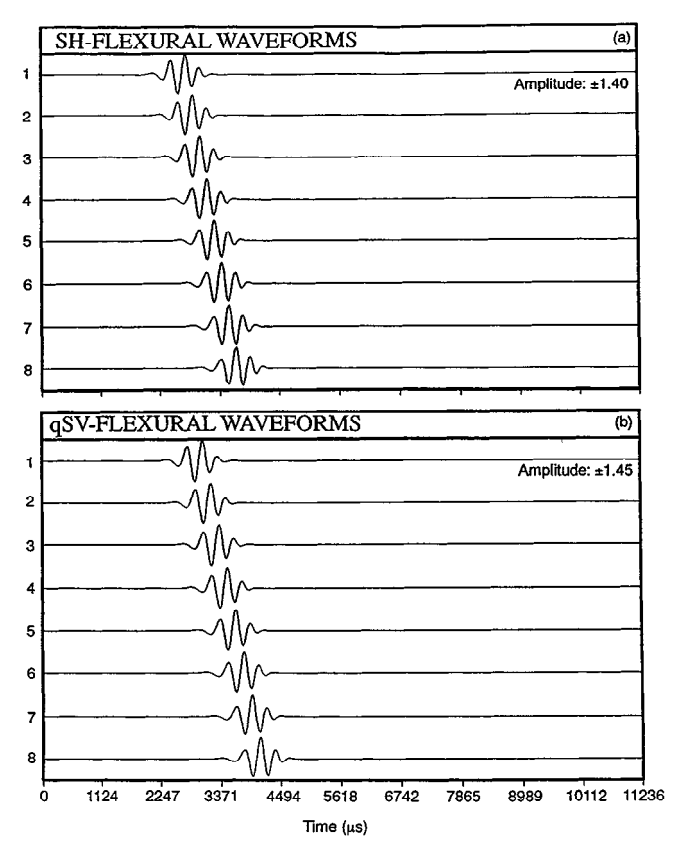


FIG. 12. (a) Synthetic waveforms caused by a dipole source directed along the *SH* wave polarization direction. Propagation direction is normal to the TI symmetry axis. (b) The same as in Figure 12a, but for the SV-polarized flexural wave.

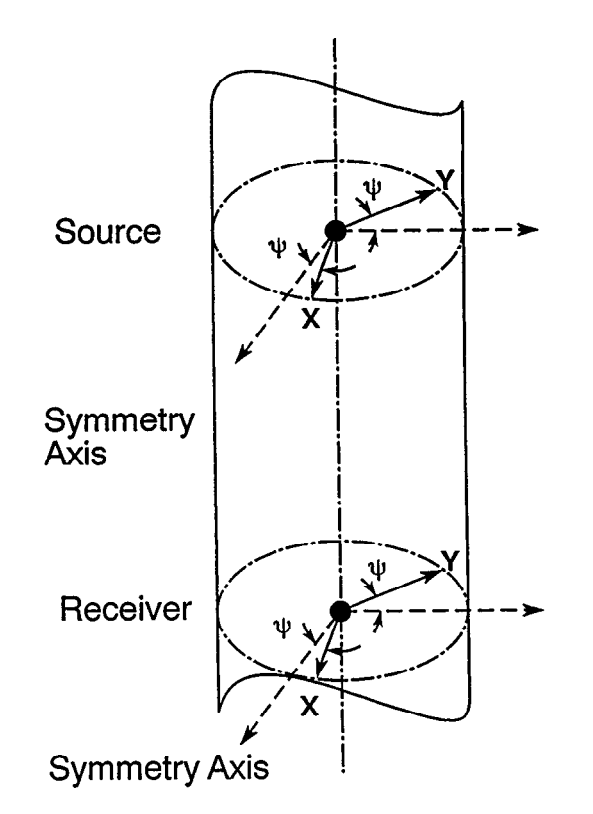


FIG. 13. Schematic diagram of orientations of a dipole source and inline or crossline receivers in a borehole.

CONCLUSIONS

We have demonstrated that proper selection of equivalent isotropic parameters for given propagation and polarization directions can greatly simplify modeling of borehole flexural waves in anisotropic formations. These equivalent parameters for the SH -polarized flexural waves are obtained from the exact qP- and SH- wave velocities; whereas those for the @V-polarized flexural waves are derived from the exact qPand qSV -wave velocities for propagation along the borehole axis. With this choice of isotropic parameters for the unperturbed solution, we have observed that the perturbative correction to the flexural wave dispersion curve is negligible for fast and slow formations considered in this study. A small perturbative correction not only ensures a greater accuracy in the prediction of the dispersion curves in the presence of anisotropic formations, but also implies that the anisotropic formation can be adequately represented in terms of two equivalent isotropic formations for the purpose of modeling the SH- and $qS\bar{V}$ -polarized borehole flexural waves. This conclusion is further supported by the observa-

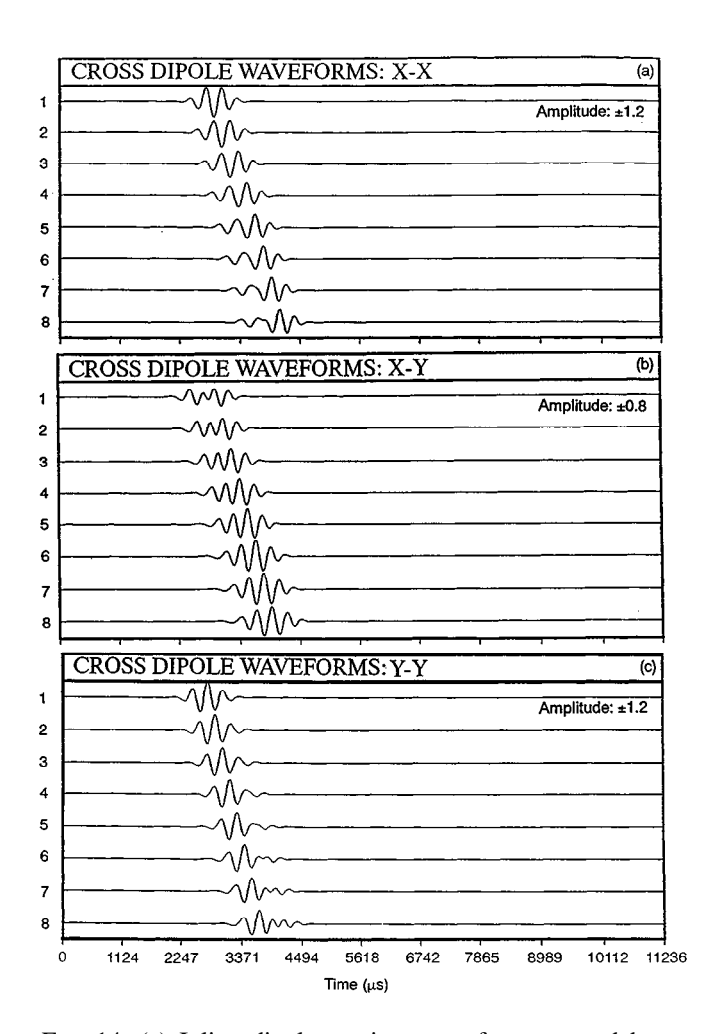


FIG. 14. (a) Inline dipole receiver waveforms caused by a dipole source directed along an azimuthal angle of 30 degrees from the TI symmetry axis. Propagation direction is normal to the symmetry axis. (b) The same as in Figure 14a, but for the crossline dipole receiver waveforms. (c) The same as in Figure 14a, but for the dipole source and receivers perpendicular to that of Figure 14a.

tion that the sagittal plane in a TI medium is also a plane of mirror symmetry. As a result, the qP- and #V-displacement components are intercoupled but independent of the SH-displacement component.

REFERENCES

Auld, B. A., 1973, Acoustic fields and waves in solids, volumes I and II: John Wiley & Sons, Inc.
Backus, G. K., 1962, Long-wave elastic anisotropy produced by horizontal layering: J. Geophys. Res., 66, 4427-4440.
Ben-Menahem, A., and Sena, A. G., 1990, Seismic source theory in stratified anisotropic media: J. Geophys. Res., 95, 15395-15427.
Benryman, J. G. 1970, Long wave elastic enjectnosi in transporsable. Berryman, J. G., 1979, Long-wave elastic anisotropy in transversely isotropic media: Geophysics, 44, 897-917.
Chan, A. K., and Tsang, L., 1983, Propagation of acoustic waves in

a fluid-filled borehole surrounded by a concentrically layered transversely isotropic formation: J. Acoust. Soc. Am., 74, 1605-

Crampin, S., 1985, Evaluation of anisotropy by shear wave splitting: Geophysics, 50, 383-411.

Ellefsen, K. H., Cheng, C. H., and Toksöz, M. N., 1991, Applications of perturbation theory to acoustic logging: J. Geophys. Res., 96, 537-549.

96, 53/-549.
Esmersoy, C., 1990, Split shear-wave inversion for fracture evaluation: 60th Ann. Internat. Mtg., Soc. Expl. Geophys., Expanded Abstracts, 1400-1403.
Garmany, J., 1988, Seismograms in stratified anisotropic media: J. Geophys. Res., 92, 365-377.
Gassman, F., 1964, Introduction to seismic traveltime methods in anisotropic media: Pure Appl. Geophys., 58, 53-1 12.
Kemer, C., Dyer, B., and Worthington, M., 1989, Wave propagation in vertical transversely isotropic medium: Field experiment

tion in vertical transversely isotropic medium: Field experiment and model study: Geophys. J. Roy. Astr. Soc., 97, 295-309. Kurkjian, A. L., 1985, Numerical computation of individual far-field arrivals excited by an acoustic source in a borehole: Geophysics, 50, 852-866.

Kurkjian, A. L., and Chang, S. K., 1983, Geometric decay of the headwaves excited by a point force in a fluid-filled borehole: 53rd Ann. Internat. Mtg., Soc. Expl. Geophys., Expanded Abstracts,

1986, Acoustic multipole sources in fluid-filled boreholes:

Geophysics, 51, 148-163.

Lang, S. W., Kurkjian, A. L., McClellan, J. H., Morris, C. F., and Parks, T. W., 1987, Estimating slowness dispersion from arrays of sonic logging waveforms: Geophysics, 52, 530-544.

Leary, P. C., Li, Y. G., and Aki, K., 1987, Observation and

modeling of fault-zone fracture seismic anisotropy, P,

SH traveltimes: Geophys. J. Roy. Astr. Soc., 91, 461-484.
Leslie, H. D., and Randall, C. J., 1992, Multipole sources in deviated boreholes penetrating anisotropic formations: Numerical and experimental results: J. Acoust. Soc. Am., 91, 12-27.
Leveille, J. P., and Seriff A. J., 1989, Borehole wave particle motion in anisotropic formations: J. Geophys. Box. 94, 7183.

motion in anisotropic formations: J. Geophys. Res., 94, 7 183-

Levin, F. K., 1979, Seismic velocities in transversely isotropic media: Geophysics, 44, 918-936.

Liu, H-L., and Randall, C., 1991, Synthetic waveforms in noncircular boreholes using boundary integral equation method: 61st Ann. Internat. Mtg., Soc. Expl. Geophys., Expanded Abstracts, 843-845

Lo, T. W., Coyner, K. B., and Toksöz, M. N., 1986, Experimental determination of elastic anisotropy of Berea sandstone, Chicopee

shale and Chelmsford granite: Geophysics, 51, 164-171.
Randall, C. J., 1991, Modes of noncircular fluid-filled boreholes in elastic formations: J. Acoust. Soc. Am., 89, 1002-1016.

Sneddon, I. N., 1951, Fourier transforms: Sections 4 and 5: Mc-Graw Hill Book Co.

Schmitt, D. P., 1989, Acoustic multipole logging in transversely isotropic poroelastic formations: J. Acoust. Soc. Am., 86, 2397-

Thomsen, L., 1986, Weak elastic anisotropy: Geophysics, 51,

Tiersten, H. F., and Sinha, B. K., 1979, A perturbation analysis of the attenuation and dispersion of surface waves: J. Appl. Phys.,

Tongtaow, C., 1982, Wave propagation along a cylindrical borehole in transversely isotropic formation: Ph.D. thesis, Colorado

Tsang, L., and Rader, D., 1979, Numerical evaluation of the

Isang, L., and Rader, D., 1979, Numerical evaluation of the transient acoustic waveform due to a point source in a fluid-filled borehole: Geophysics, 44, 1706-1720.

Vernik, L., and Nur, A., 1991, Ultrasonic velocity and anisotropy of some petroleum source rocks: The Bakken formation, Williston Basin, N. Dakota: Stanford University Report.

White, J. E., 1983, Underground sound: Elsevier Science Publ. Co., Inc.

Inc. White, J. E., and Tongtaow, C., 1981, Cylindrical waves in trans-

versely isotropic media: J. Acoust. Soc. Am., 70, 1147-1 155. Winterstein, D. R., 1986, Anisotropic effects in P-wave and SH-wave stacking velocities containing information on lithology: Geophysics, 51, 661-672.

1987, Invited introductory paper: Shear waves in exploration: A perspective: 57th Ann. Internat. Mtg., Soc. Expl. Geophys., Expanded Abstracts, 638-641.

APPENDIX A PERTURBATION MODEL

Different ways of deriving perturbation models for elastodynamic problems have been reported (Auld, 1973; Tiersten and Sinha, 1979; Ellefsen et al., 1991). Here we present a simple derivation of a perturbation model specifically adapted for the waves propagating along a borehole. Before considering the specific problem of the borehole, we summarize some general results for an arbitrary volume V of anisotropic elastic material bounded by the surface \mathcal{G} .

We assume that the reference unperturbed state of the general medium is governed by the equations of motion

$$C_{ijk\ell}^{0}u_{k,j\ell}^{0} + \rho^{0}\omega^{0}u_{i}^{0} = 0, \quad \text{in } \mathcal{V},$$
 (A-1)

where u_i^0 denotes a harmonic solution at ω^0 , and ρ^0 is the mass density in the unperturbed state. A superscript 0 refers all quantities to the unperturbed state. The unperturbed elasticity tensor is

$$C_{ijk\ell}^{0} = \lambda \delta_{ij} \delta_{k\ell} + \mu (\delta_{ik} \delta_{j\ell} + \delta_{i\ell} \delta_{jk}), \qquad (A-2)$$

and λ and μ are the Lame constants of the equivalent isotropic medium. The self-adjoint boundary conditions on

the bounding surface ${\mathcal G}$ are such that either the traction $n_i C_{iik\ell}^0 u_{k,\ell}^0$ or the displacement u_i^0 vanishes on \mathcal{G} . The corresponding equations of motion in the perturbed state are

$$C_{ijk\ell} u_{k,j\ell} + \rho \omega^2 u_i = 0, \quad \text{in } \mathcal{V},$$
 (A-3)

and the associated boundary conditions on $\mathcal G$ are such that either $n_i C_{ijk\ell} u_{k,\ell}$ or u_i vanishes. The elastic constants $C_{ijk\ell}$ and mass density ρ , respectively, in the perturbed state are assumed to take the form

$$C_{ijk\ell} = C_{ijk\ell}^0 + \varepsilon C'_{ijk\ell}, \qquad (A-4)$$

and

$$\rho = \rho^0 + \epsilon \rho'. \tag{A-5}$$

Here ε is a small positive number, $\varepsilon \ll 1$, which is introduced to simplify the asymptotic analysis. Its actual value is immaterial, but its order of magnitude is characterized by the relative difference between the perturbed and unperturbed parameters. Generally speaking, the small perturbation parameter ε defined by the relative difference between the

perturbed elastic constants $C_{ijk\ell}$ and unperturbed elastic constants $C_{ijk\ell}^0$ should be less than 0.1. However, the small perturbation parameter in this context depends on the choice of the unperturbed elastic constants, and it differs from weak material anisotropy as defined by Thomsen (1986). While the small perturbation parameter may be made progressively smaller by selecting the unperturbed elastic constants closer to the perturbed constants, weak material anisotropy parameters are fixed for a given material. A solution to the equation of motion (A-3) with the self-adjoint boundary conditions in the perturbed state may be expressed as

$$u_i = u_i^0 + \varepsilon v_i, \tag{A-6}$$

and

$$\omega = \omega^0 + \varepsilon \omega'. \tag{A-7}$$

Taking the inner product of equation (A-3) with u_i^* , integrating over the volume \mathcal{V} , using the perturbational expressions in equations (A-4) to (A-7), and keeping terms up to ε^1 order of approximation, we obtain

$$\int_{\mathcal{V}} d\mathcal{V} [C_{ijk\ell} u_{k,j\ell} + \rho \omega^{2} u_{i}] u_{i}^{*} = \int_{\mathcal{V}} d\mathcal{V} [C_{ijk\ell}^{0} u_{k,j\ell}^{0} u_{i}^{0} + \rho^{0} \omega^{0} u_{i}^{0} u_{i}^{0*} + \varepsilon C'_{ijk\ell} u_{k,j\ell}^{0} u_{i}^{0*} + \varepsilon \rho^{0} 2 \omega^{0} \omega' u_{i}^{0} u_{i}^{0*} + \varepsilon \rho'^{0} 2 \omega^{0} u_{i}^{0} u_{i}^{0*} + \varepsilon \rho'^{0} 2 \omega'^{0} u_{i}^{0*} u_{i}^{0*} u_{i}^{0*} + \varepsilon \rho'^{0} 2 \omega'^{0} u_{i}^{0*} u_{i}^{0*} u_{i}^{0*} + \varepsilon \rho'^{0} 2 \omega'^{0} u_{i}^{0*} u_{$$

where * denotes complex conjugate.

The first two terms in the integrand of the right-hand side vanish according to equation (A-l). The last three terms simplify as shown below

$$\epsilon \int_{\mathcal{V}} d\mathcal{V} [C^{0}_{ijk\ell}(v_{k,j\ell}u_{i}^{0*} + u_{k,j\ell}^{0}v_{i}^{*}) + 2\rho^{0}\omega^{0^{2}}u_{i}^{0}v_{i}^{*}]
= \epsilon \int_{\mathcal{V}} d\mathcal{V} C^{0}_{ijk\ell}(v_{k,j\ell}u_{i}^{0*} + u_{k,j\ell}^{0}v_{i}^{*} - 2u_{k,j\ell}^{0}v_{i}^{*})
= \epsilon \int_{\mathcal{V}} d\mathcal{V} C^{0}_{ijk\ell}(v_{k,j\ell}u_{i}^{0*} - u_{k,j\ell}^{0}v_{i}^{*})
= \epsilon \int_{\mathcal{V}} d\mathcal{V} C^{0}_{ijk\ell}(v_{k,j\ell}u_{i}^{0*} - u_{k,j\ell}^{0}v_{i}^{*})$$
(A-9)

In deriving equation (A-9), we have used equation (A-1) in the first equality, and the divergence theorem along with the unperturbed traction free boundary conditions on the bounding surface \mathcal{G} in the last equality. The remaining terms in equation (A-8) along with equation (A-9) then take the form

$$\varepsilon \int_{\mathcal{S}} d\mathcal{S} n_j C^0_{ijk\ell} v_{k,\ell} u_i^{0*} + \varepsilon \int_{\mathcal{V}} d\mathcal{V} [C'_{ijk\ell} u_{k,j\ell}^{0} u_i^{0*}]$$

$$+2\rho^0\omega^0\omega'u_i^0u_i^{0*}+\rho'\omega^0u_i^2u_i^0u_i^{0*}]=0.$$
 (A-10)

Integrating the first term by parts, then applying the divergence theorem and boundary conditions on the bounding surface $\mathcal G$ in the perturbed state, we obtain

$$\omega' = \frac{\int_{\mathcal{V}} d\mathcal{V} C'_{ijk\ell} u^{0}_{k,\ell} u^{0*}_{i,j}}{2\omega^{0} \int_{\mathcal{V}} d\mathcal{V} \rho^{0} u^{0}_{i} u^{0*}_{i}} - \frac{\omega^{0} \int_{\mathcal{V}} d\mathcal{V} \rho' u^{0}_{i} u^{0*}_{i}}{2 \int_{\mathcal{V}} d\mathcal{V} \rho^{0} u^{0}_{i} u^{0*}_{i}}.$$
 (A-11)

For a circular borehole of radius *a*, which is invariant along the axial z-direction, we can write the displacement field in the following separable form

$$\mathbf{u}^{0}(r, \phi, z) = \hat{\mathbf{u}}^{0}(r, \phi)e^{ikz}. \tag{A-12}$$

Equation (A-l 1) can now be written explicitly in the cylindrical coordinates for waves propagating along the borehole, and noting the periodicity of the solution along the axial direction.

$$\omega' = \frac{\int_{a}^{\infty} r \, dr \int_{0}^{2\pi} d\phi [C'_{ijk\ell} u^{0}_{i,j} u^{0}_{k,\ell}^{*} - \rho' \omega^{0} u^{0}_{i} u^{0}_{i}^{*}]}{2\omega^{0} \left[\rho_{f} \int_{0}^{a} r \, dr \int_{0}^{2\pi} u^{f}_{i} u^{f*}_{i} \, d\phi + \rho^{0} \int_{a}^{\infty} r \, dr \int_{0}^{2\pi} u^{0}_{i} u^{0}_{i}^{*} \, d\phi \right]},$$
(A-13)

where u_i^f is the displacement in the borehole liquid of mass density ρ_f . The perturbed material parameters in equation (A-1 1) or" equation (A-13) may have arbitrary dependence upon both r and ϕ , as long as the perturbation is small. The procedure for applying equation (A-13) to borehole modes in anisotropic formations ($C'_{iik\ell} \neq 0$, $\rho' = 0$) is discussed in detail in Appendix B. For each value of the axial wavenumber k (see Appendix B and below) the unperturbed mode u_i^0 is first obtained. Then the integrals in equation (A-13) are performed to give the frequency perturbation ω' . These are added to the eigenfrequency ω^0 for various values of k to obtain the final dispersion curves for the anisotropic case.

The phase slowness dispersion curves may also be readily obtained by expressing the slowness perturbation in terms of the frequency perturbation at a given wavenumber. Let the unperturbed modal phase slowness be S^0 and the actual phase slowness be $S^0 + \varepsilon S'$ at a given wavenumber k. Then

$$k = \omega^0 S^0 = (\omega^0 + \varepsilon \omega')(S^0 + \varepsilon S'), \qquad (A-14)$$

which yields the following relationship between the slowness and frequency perturbations at a given wavenumber

$$S' = -\frac{S^0}{\omega^0} \omega', \tag{A-15}$$

where terms of order higher than ϵ are neglected.

The analysis in Appendices B and C is for modes of arbitrary azimuthal order $n \ge 0$ although our interest here is is primarily for the flexural mode n = 1. Appendix B discusses the modes and provides an outline of the evaluation of the perturbation integrals in the numerator of equation (A-13). In particular, closed form expresisions are given for the ϕ integration of the flexural wave solution in cylindrical coordinates. Closed form expressions for the integrals in the denominator are given in Appendix C.

APPENDIX B

THE PERTURBATION INTEGRAL IN CYLINDRICAL COORDINATES

Since the unperturbed solution in the axisymmetric case is known in terms of cylindrical functions, it is expedient to carry out the volume integrals appearing in the perturbation result in equation (A-13) in cylindrical coordinates. To this end, we first note that

$$\int_{r>a} dA C'_{ijk\ell} u_{i,j} u_{k,\ell} = \int_{r>a} dA C'_{ijk\ell} e_{ij} e_{k\ell}, \qquad (B-1)$$

where the strain tensor $e_{ij} = \frac{1}{2} (u_{i,j} + u_{j,i})$, and the equality is justified because of the symmetry of the second-order elastic constants $C'_{ijk\ell}$. The integration in equation (B-l) is conveniently performed in cylindrical coordinates r and ϕ . The r-integral cannot, in general, be simplified. However, the \$-integral may be explicitly performed, which we now demonstrate.

We first transform the strain into cylindrical coordinates. It may be shown that the six strain components for a borehole wave of nth order in the circumferential parameter ϕ can be expressed in separable form,

$$\mathbf{e} = \mathbf{T}_n(\mathbf{\phi})\mathbf{E}(r),$$
 (B-2)

where ϕ is the rotation of the radial direction about the borehole axis; the six vectors e and E are, respectively

$$\mathbf{e}^{t}(r, \, \phi) = [e_{rr}e_{\phi\phi}e_{zz}2e_{\phi z}2e_{rz}2e_{r\phi}],$$
 (B-3)

$$\mathbf{E}^{t}(r) = [E_{rr}E_{\phi\phi}E_{zz}E_{\phi z}E_{rz}E_{r\phi}], \qquad (B-4)$$

where the superscript t denotes transpose, and

 $\mathbf{T}_n(\mathbf{\phi})$

= diag [$\cos n\phi \cos n\phi \cos n\phi \sin n\phi \sin n\phi \cos n\phi$].

(B-5)

The representation of the moduli in cylindrical coordinates can be achieved by rotating the coordinate system with 4. Thus, when 4 = 0, the components in the cylindrical and Cartesian coordinate systems coincide with r, 4 and z directions being parallel to the axes x_1' , x_2' , and x_3' of Figure 1, respectively. The original elements of $C(6 \times 6)$ in this system are assumed to be of arbitrary anisotropic form, i.e., as many as 21 independent elements. These transform with 4 into the following form in the rotated frame,

$$\underline{\mathbf{C}}' = \underline{\mathbf{Q}}\underline{\mathbf{C}}\underline{\mathbf{Q}}^t, \tag{B-6}$$

where the elements of $Q(6 \times 6)$ are (Auld, 1973)

$$\mathbf{Q} = \begin{bmatrix} \cos^2 \phi & \sin^2 \phi & 0 & 0 & 0 & \sin 2\phi \\ \sin^2 \phi & \cos^2 \phi & 0 & 0 & 0 & -\sin 2\phi \\ 0 & 0 & 1 & 0 & 0 & 0 \\ 0 & 0 & 0 & \cos \phi & -\sin \phi & 0 \\ 0 & 0 & 0 & \sin \phi & \cos \phi & 0 \\ -\frac{1}{2}\sin 2\phi & \frac{1}{2}\sin 2\phi & 0 & 0 & \cos 2\phi \end{bmatrix}$$
(B-7)

Equation (B-6) represents the elastic moduli \mathbf{C}' in polar coordinates.

Since the ϕ dependence of both $C'_{ijk\ell}$ and e_{ij} are now known, we can carry out the ϕ integration analytically. The surface integral in the $r - \phi$ plane can now be expressed as

$$\int_{0}^{2\pi} d\phi \int_{a}^{\infty} r \, dr \, e_{ij} C'_{ijk\ell} e^{*}_{k\ell}$$

$$= 2\pi \int_{0}^{\infty} r \, dr \, \mathbf{E}^{t}(r) \mathbf{C}'' \mathbf{E}^{*}(r), \quad (B-8)$$

where * denotes complex conjugate, and it is assumed that the complex form of solution is employed. The constant matrix **C**" is defined by

$$\underline{\mathbf{C}}'' = \frac{1}{2\pi} \int_0^{2\pi} d\phi \ \underline{\mathbf{T}}_n \underline{\mathbf{C}}' \underline{\mathbf{T}}_n. \tag{B-9}$$

Explicit integration implies that the elements of $C''(6 \times 6)$ have the values

$$C_{11}^n = C_{11}G_1^n + C_{22}G_2^n + 2(C_{12} + 2C_{66})G_3^n,$$
 (B-10)

$$C_{12}^{"} = C_{12}(G_1^n + G_2^n) + (C_{11} + C_{22} - 4C_{66})G_3^n,$$
 (B-11)

$$C_{13}^{"} = C_{13}F_1^n + C_{23}F_2^n,$$
 (B-12)

$$C_{16}^{"} = (C_{12} - C_{11} + 2C_{66})G_7^n$$

+
$$(C_{22} - C_{12} - 2C_{66})G_8^n$$
, (B-13)

$$C_{22}^{"} = C_{22}G_1^n + C_{11}G_2^n + 2(C_{12} + 2C_{66})G_3^n,$$
 (B-14)

$$C_{23}^{"} = C_{23}F_1^n + C_{13}F_2^n,$$
 (B-15)

$$C_{26}^{"} = (C_{22} - C_{12} - 2C_{66})G_7^n$$

$$+ (C_{12} - C_{11} + 2C_{66})G_8^n,$$
 (B-16)

$$C_{33}'' = C_{33}(0.5 + 0.5\delta_{n0}),$$
 (B-17)

$$C_{36}'' = \frac{1}{8} (C_{23} - C_{13}) \delta_{n1},$$
 (B-18)

$$C_{44}'' = C_{44}F_3^n + C_{55}F_4^n,$$
 (B-19)

$$C_{45}'' = (C_{44} - C_{55})F_5^n,$$
 (B-20)

$$C_{55}^{"} = C_{55}F_1^n + C_{44}F_2^n,$$
 (B-21)

$$C_{66}^{"} = C_{66}(G_4^n + G_5^n) + (C_{11} + C_{22} - 2C_{12} - 2C_{66})G_6^n,$$
 (B-22)

and

$$C''_{14} = C''_{15} = C''_{24} = C''_{25} = C''_{34} = C''_{35} = C''_{46} = C''_{56} = 0.$$
(B-23)

The F and G quantities are obtained from the ϕ integrals in equation (B-9) and are

$$F_{1}^{n} = \frac{1}{4} + \frac{1}{4} \, \delta_{n0} + \frac{1}{8} \, \delta_{n1} \,,$$

$$F_{2}^{n} = F_{1}^{n} - \frac{1}{4} \, \delta_{n1} \,, \quad F_{3}^{n} = \frac{1}{2} - F_{1}^{n} \,, \quad F_{4}^{n} = F_{1}^{n} - \frac{1}{2} \, \delta_{n0} \,,$$

$$G_{1}^{n} = \frac{3}{16} + \frac{3}{16} \, \delta_{n0} + \frac{1}{8} \, \delta_{n1} + \frac{1}{32} \, \delta_{n2} \,,$$

$$G_{2}^{n} = G_{1}^{n} - \frac{1}{4} \, \delta_{n1} \,, \quad G_{3}^{n} = F_{1}^{n} - G_{1}^{n} \,, \quad G_{4}^{n} = \frac{3}{8} - G_{1}^{n} \,,$$

$$G_{5}^{n} = \frac{3}{8} + \frac{1}{4} \, \delta_{n1} - G_{1}^{n} \,, \quad G_{6}^{n} = \frac{1}{16} - \frac{1}{16} \, \delta_{n0} + \frac{1}{32} \, \delta_{n2} \,,$$

$$G_{7}^{n} = -\frac{1}{32} \, \delta_{n0} + \frac{1}{16} \, \delta_{n1} + \frac{1}{32} \, \delta_{n2} \,,$$

$$G_{8}^{n} = \frac{1}{33} \, \delta_{n0} + \frac{1}{16} \, \delta_{n1} - \frac{1}{32} \, \delta_{n2} \,. \quad (B-24)$$

For the particular case of the flexural mode (n = 1), these become

$$F_{1}^{1} = F_{4}^{1} = \frac{3}{8}, \quad F_{2}^{1} = F_{3}^{1} = F_{5}^{1} = \frac{1}{8},$$

$$G_{1}^{1} = G_{5}^{1} = \frac{5}{16},$$

$$G_{2}^{1} = G_{3}^{1} = G_{4}^{1} = G_{6}^{1} = G_{7}^{1} = G_{8}^{1} = \frac{1}{16}.$$
(B-26)

We note that the matrix \mathbf{C}'' is generally monoclinic with respect to the z-direction and independent of the "non-monoclinic" elements of \mathbf{C} , i.e., the same elements that occur in equation (B-23). In addition, \mathbf{C}'' does not depend upon the moduli C_{16} , C_{26} , C_{36} , and C_{45} , but only on the nine "orthorhombic" elements of \mathbf{C} .

We close this Appendix with a discussion of the elements of the r-dependent six components of vector \mathbf{E} of equation (B-4). The strains in equation (B-4) are obtained from the complex representation of the flexural wave solution, which may be written in the form

$$u_{r} = \left[\left(\frac{n}{r} H_{n}(k_{1}r) - k_{1} H_{n+1}(k_{1}r) \right) A + i k_{z} H_{n+1}(k_{2}r) A_{1} + \frac{n}{r} H_{n}(k_{2}r) A_{3} \right] \cos n \phi e^{ikz}, \quad (B-27)$$

$$u_{\phi} = \left[-\frac{n}{r} H_n(k_1 r) A + ik H_{n+1}(k_2 r) A + \left(k_2 H_{n+1}(k_2 r) - \frac{n}{r} H_n(k_2 r) \right) A_3 \right] \sin n\phi e^{ikz},$$
(B-28)

$$u_z = [ikH_n(k_1r)A - k_2H_n(k_2r)A_1] \cos n\phi e^{ikz},$$
 (B-29)

where n = 1 for the flexural wave solution, $H_n(x)$ represents Hankel function of the first kind and of order n, which

is consistent with the outgoing waves for the assumed time dependence of ${\rm e}^{-i\omega t}$. The radial wavenumbers k_1 and k_2 are given by

$$k_1^2 = \frac{\omega^2}{V_1^2} - k^2,$$
 (B-30)

$$k_2^2 = \frac{\omega^2}{V_2^2} - k^2,$$
 (B-31)

where V_1 and V_2 are the qP and qSV- (or SH-) wave velocities along the borehole axis for the SV- (or SH-) polarized flexural waves. The associated flexural wave solution in the borehole fluid may be written as

$$u_r^f = A^f \left[\frac{n}{r} J_n(k_r r) - k_r J_{n+1}(k_r r) \right] \cos n\phi e^{ikz},$$
 (B-32)

$$u_{\phi}^{f} = -\frac{n}{r} J_{n}(k_{r}r)A^{f} \sin n\phi e^{ikz}, \qquad (B-33)$$

$$u_z^f = ikJ_n(k_r r)A^f \cos n\phi e^{ikz}, \qquad (B-34)$$

where the superscript f refers the quantity to the borehole fluid, and k_r is given by

$$k_r^2 = \frac{\omega^2}{c_f^2} - k^2,$$
 (B-35)

and c_f is the compressional-wave velocity in the borehole fluid.

The radial displacement coefficients for u_r , u_{ϕ} , and u_z in the formation and borehole fluid are given by the quantities in square brackets of equations (B-27 to B-29) and equations (B-32 to B-34), respectively. The associated radial stress coefficients for σ_{rr} , $\sigma_{\phi\phi}$, and ϕ_{zz} are similarly defined by collecting the radial functional dependence of these stress components.

The amplitude coefficients A^f , A, A_1 , and A_3 are obtained from the four continuity conditions at the borehole surface r = a. The four continuity conditions at r = a are

$$u_r = u_r^f, (B-36)$$

$$\sigma_{rr} = \sigma_{rr}^f, \tag{B-37}$$

$$\sigma_{r\phi} = 0, \tag{B-38}$$

$$\sigma_{rz} = 0. (B-39)$$

Equations (B-36 to B-39) constitute a system of four linear homogeneous algebraic equations in the wave amplitudes A^f , A, A_1 , and A_3 , which yields nontrivial solutions when the determinant of the coefficients of the wave amplitudes vanishes. The solution, and the corresponding relationship between k and ω , is obtained numerically for a given modal propagation.

APPENDIX C

THE NORMALIZATION INTEGRAL

In this Appendix we give a closed form expression for the integral that occurs in the denominator of equation (A-13) and also in the definition of M^m in equation (14). The integral may be separated into separate integrals in the fluid and solid. The former follows simply from the definition of \mathbf{u}^f in Appendix A as

$$\int_{0}^{a} r \, dr \int_{0}^{2\pi} d\phi \mathbf{u}^{f} \cdot \mathbf{u}^{f*}$$

$$= \pi \gamma_{n} |A^{f}|^{2} \left[J_{n}(k_{r}a)[k_{r}aJ_{n-1}(k_{r}a) - nJ_{n}(k_{r}a)] + \frac{1}{2} \left(\frac{\omega a}{c_{f}} \right)^{2} [J_{n}^{2}(k_{r}a) - J_{n-1}(k_{r}a)J_{n+1}(k_{r}a)] \right], \quad (C-1)$$

where $\gamma_n \equiv 1 + \delta_{n0}$. The remaining integral is more complicated, but can be simplified using the following identity for the elastic displacement field in an isotropic solid

$$\mathbf{u} = \nabla \mathbf{\phi} + \nabla \times \mathbf{H},\tag{C-2}$$

where 4 is a compressional potential, and H a vector shear potential. Assuming time harmonic motion, each of these potentials satisfies a corresponding Helmholtz equation. Let V be an arbitrary volume with surface S and outward normal n. Then it can be shown that

$$\int_{V} \mathbf{u} \cdot \mathbf{u}^{*} dV = \frac{\omega^{2}}{V_{1}^{2}} \int_{V} \phi \phi^{*} dV + \frac{\omega^{2}}{V_{2}^{2}} \int_{V} \mathbf{H} \cdot \mathbf{H}^{*} dV$$

$$- \int_{V} (\nabla \cdot \mathbf{H}) (\nabla \cdot \mathbf{H})^{*} dV + \int_{S} \left[\phi^{*} \frac{\partial \phi}{\partial n} + \mathbf{H}^{*} \cdot \frac{\partial \mathbf{H}}{\partial n} \right]$$

$$- \mathbf{n} \cdot (\mathbf{H}^{*} \cdot \nabla) \mathbf{H} + \mathbf{n} \cdot \mathbf{H}^{*} (\nabla \cdot \mathbf{H}) dS$$

$$+ \int_{S} \left[2 \operatorname{Re} \left[\phi^{*} \mathbf{n} \cdot (\nabla \times \mathbf{H}) \right] dS. \qquad (C-3)$$

Applying this to the integral in the formation, we find

$$\frac{1}{\pi} \int_{a}^{\infty} r \, dr \int_{0}^{2\pi} d\phi \mathbf{u} \cdot \mathbf{u}^{*}$$

$$= \frac{\omega^{2}}{V_{1}^{2}} \left| \frac{A}{k_{1}} \right|^{2} \gamma_{n} I_{n}(k_{1}a) + \frac{\omega^{2}}{V_{2}^{2}} \left| \frac{A_{1}}{k_{2}} \right|^{2} 2 I_{n+1}(k_{2}a)$$

$$+ \left(\frac{\omega^{2}}{V_{2}^{2}} \left| \frac{c_{3}}{k_{2}} \right|^{2} - \left| A_{1} + ic_{3} \frac{k}{k_{2}} \right|^{2} \right) \bar{\gamma}_{n} I_{n}(k_{2}a)$$

$$- |A|^{2} \gamma_{n} L_{n}(k_{1}a) - |A_{1}|^{2} \gamma_{n} L_{n+1}(k_{2}a)$$

$$- |c_{3}|^{2} \bar{\gamma}_{n} L_{n}(k_{2}a) - (1+n) \gamma_{n} |h_{1}|^{2} - |k_{1}a| \bar{\gamma}_{n} h_{1} h_{3}^{*}$$

$$- \bar{\gamma}_{n} a \left(\frac{c_{1}k_{2}}{c_{3}} + ik \right) h_{1}^{*} h_{3}$$

$$+ 2 \gamma_{n} \operatorname{Re} \left[\frac{A^{*}}{c_{3}^{*}} h_{3}^{*}(nh_{3} + ikah_{1}) \right], \qquad (C-4)$$

where $\bar{\gamma}_n = 1 - \delta_{n0}$,

and

$$c_{3} = A_{3} - i \frac{k}{k_{2}} A_{1},$$

$$h_{1} = A_{1} H_{n+1}(k_{2} a),$$

$$h_{3} = c_{3} H_{n}(k_{2} a),$$

$$L_{n}(x) = H_{n}^{*}(x) [nH_{n}(x) - xH_{n+1}(x)],$$

$$I_{n}(x) = (-1)^{n} \frac{|x|^{2}}{2} [H_{n}^{2}(x) - H_{n+1}(x)H_{n-1}(x)].$$

Note that both k_1 and k_2 are assumed to be purely imaginary in these equations.

APPENDIX D

THE DIPOLE SOURCE SPECTRUM

The equations of motion in the borehole fluid may be given by

$$\nabla^2 \mathbf{u}^f + k_f^2 \mathbf{u}^f = -\mathscr{F}_0(\omega)/\lambda_f, \qquad (D-1)$$

where the subscript or superscript "f" refers the quantity to the fluid, $\mathcal{F}_0(\omega)$ is the forcing function density, $\lambda_f = \rho_f c_f^2$ is the bulk modulus of the fluid, and $k_f = \omega/c_f$. The forcing function $\mathcal{F}_0(\omega)$ for a monopole and dipole sources are, respectively, given by Kurkjian and Chang (1986)

$$\mathcal{F}_0(\omega) = -\lambda_f V_0(\omega) \nabla \delta(x),$$

for a monopole source, (D-2)

and

$$\mathcal{F}_0(\omega) = -\lambda_f \delta V_0(\omega) \hat{\mathbf{e}}_{\beta} . \nabla \nabla \delta(x),$$
 for a dipole source, (D-3)

where $\hat{\mathbf{e}}_{\beta}$ is a unit vector directed along the dipole direction oriented at an angle β from the reference x_2 -axis in the borehole cross-sectional plane, and the constant δ (not to be confused with the Dirac delta function) is the multipole separation parameter in meters.

To evaluate $\mathcal{F}_0(\omega)$, the forcing term in equation (21), we note that the modal displacement field \mathbf{U}^m in the borehole fluid is equal to the fluid displacement field \mathbf{u}^f ,

which may be expressed in terms of a displacement potential ϕ^m given by

$$\mathbf{u}^f = \nabla \phi^m = \nabla A^f J_m(k_f r) \cos m\phi, \quad m = 1,$$
 for a flexural mode, (D-4)

where

$$\nabla = \hat{\mathbf{e}}_{\mathbf{r}} \frac{\partial}{\partial r} + \hat{\mathbf{e}}_{\phi} \frac{\partial}{r \partial \phi}, \qquad (D-5)$$

and $J_{n}(x)$ denote the Bessel function of the first kind of order m. Substitution of equations (D-3) and (D-4) into the expression within the square-bracket of equation (19), yields

$$\begin{split} \mathcal{F}_0(\omega) \cdot \mathbf{U}^{m*}(0, \ k_m(\omega)) \\ &= -\rho_f \omega^2 V_0(\omega) k_f \delta \pi \cos \beta A^{f*} \delta_{m1}, \quad \text{(D-6)} \end{split}$$

where β represents the dipole orientation from the reference axis, * denotes complex conjugate, and $(k_f\delta)$ and $V_0(\omega)$ represent the strength and frequency spectrum of the dipole transmitter.